

A Diffusion Model for Classical Chaotic Compound Scattering

F. Leyvraz^{a,b}, M. Lombardi^{a,c,1} and T.H. Seligman^{a,b}

^a*Centro Internacional de Ciencias, Cuernavaca, Mexico*

^b*Centro de Ciencias Físicas, UNAM, Av. Universidad s/n, Col. Chamilpa, Morelos, Mexico*

^c*Laboratoire de Spectrométrie Physique (CNRS UMR 5588), Université Joseph-Fourier de Grenoble, BP87, F-38402 Saint Martin d'Hères Cédex, France*

Abstract

We consider the classical map proposed previously to be the exact classical analog of Rydberg Molecules calculated with the approximations relevant to the multi-channel quantum defect theory. The resulting classical map is analyzed at energies above the threshold for the Rydberg electron. At energies very near to this threshold we find the possibility of bounded motion for positive energy due to conserved tori as well as the possibility of forming a compound system, i.e. a system where the particle is trapped for long times before emerging again to the continuum. The compound scattering displays unusual features for short time behavior. A diffusion model explains these features.

Key words: Chaotic scattering, Rydberg Molecule, Diffusion Model.

PACS: 5.45.Ac, 33.80.Rv, 24.60.Dr

1 Introduction

The Multichannel Quantum Defect Theory (MQDT) is a well established quantum approximation framework to accurate spectroscopic studies of atoms [1] and molecules [2] near (*i.e.* both below and above) an ionization limit. More recently the MQDT theory for molecules has been used as an interesting tool to test ideas about the quantum signatures of classical chaos [3–5]. Since this

¹ Corresponding author; Fax: +33 476 514 544; e-mail: Maurice.Lombardi@ujf-grenoble.fr

correspondence is valid only near the semi classical limit, *i.e.* for large quantum numbers, some of these these quantum numbers have been taken much larger than their usual experimental values. To simplify the mathematical analysis, an approximation (the conservation of the angular momentum L of the outer (Rydberg) electron) valid in the case of usual small molecules only for low L has been kept for much higher values of L . Indeed we apply a low- L – approximation in the semi-classical limit, *i.e.* for large L . Other approximations better suited to actual small molecules have been used in recent calculations [6]. A possible experimental way out is to study much larger molecules, and this is not out of reach since recent experimental studies have found Rydberg states on molecules as large as Benzene Argon complexes[7], Diazacyclooctane (DABCO) and bis (benzene) chromium (BBC)[8]. These experimental studies however involve other issues, namely the vibrational transfers between the very dense set of vibrational levels of such large molecules. While all these experimental issues are very interesting to study, we will not consider them in this paper.

We will use the model only for its interesting theoretical properties with respect to the problem at hand, namely the study of chaotic scattering. Indeed one of us (M.L.) with co workers proposed a classical map, the quantization of which is exactly solved by the MQDT [3]. This approximate system deserves to be studied for its own sake precisely because we can compute the corresponding quantum results without approximation. The study of the correspondence between classical and quantum results, however, will be deferred to future work. In the present paper we establish only interesting classical results. With this proviso we shall in this paper refer to the approximate classical system as the Rydberg molecule.

The Rydberg molecule provides a remarkably simple example of a two dimensional system that displays compound behavior and positive energy bound states typical of many-body systems. It will therefore be of interest to study its scattering functions.

Among the classical scattering functions the time delays are commonly used as they display the singularity structure of such functions very clearly and simultaneously have an intuitive meaning. The number of iterations of an internal Poincaré map are a convenient alternative to time delays that does not reflect distortions by far flung trajectories that are particularly important in the Coulomb case. As we are precisely in this situation we shall mainly use the latter, though we shall also display the mentioned distortions. The results for the number of iterations display a very surprising structure of successive decay laws. We cannot hope to obtain an understanding by reconstructing the chaotic saddle. Indeed we have not been able to resolve the fractal structure of the scattering functions and therefore no branching tree was obtained. The reason was precisely the complexity induced by the far flung trajectories, which

produce much too narrow structures (see the discussion at the beginning of sec. 3). We therefore develop a diffusive model that reflects this situation and can be qualitatively related to the dynamical behavior of our system.

2 The Classical Model

In ref. [3] the Rydberg molecule is described classically as a map of the unit sphere onto itself. This sphere corresponds to the orientations of the orbital angular momentum \vec{L} of the electron (whose absolute value is approximated to be constant) after each collision with the molecular core. The construction of the map and its description turn out to be somewhat involved. Conceptually, the simplest approach seems to be that of looking at the system in the laboratory frame. The final results will be stated in a form that is essentially frame independent.

We define a unit vector \vec{P} in the direction of the core axis, the electron angular momentum \vec{L} , the core angular momentum \vec{N} and the electronic energy E_e . This yields a total of seven quantities. (We do not consider the quantities \vec{P} , since they are determined up to an initial condition by the time evolution of \vec{N} which is perpendicular to \vec{P} .) Between these seven quantities, there exist five relations given by total energy (E) conservation, the conservation of total angular momentum

$$\vec{J} = \vec{L} + \vec{N} \quad (1)$$

and finally, the approximate conservation of the magnitude of the electronic angular momentum L . From this follows that one only needs two numbers to specify fully the configuration of the system once total energy, total angular momentum and L are known. For these we choose the two polar angles θ and ϕ determining the relative orientation of \vec{L} with respect to \vec{P} as polar axis and \vec{N} as reference axis for ϕ or, alternatively, the angles α and β determining the orientation of \vec{L} with respect to \vec{N} and Y (see fig. 1). As a matter of notation, we define $R_{\vec{a}}(\psi)$ to be a rotation of angle ψ around the axis \vec{a} in the positive direction. We are now ready to define the two basic components of the map: All quantities with an index n refer to a given time step, whereas primed quantities are intermediate quantities for computation only. We therefore aim to express such quantities as \vec{L}_{n+1} in terms of \vec{L}_n .

- (1) Free Keplerian motion: When the electron is far from the core, it feels only the isotropic $1/r$ potential of the core and thus follows a free Coulomb trajectory, so that its angular momentum \vec{L} is fixed. The core on the other hand, feels no torque from the electron and thus performs a free rotation. This implies for \vec{L} , \vec{N} and \vec{P} the following evolution:

$$\begin{aligned}
\vec{L}' &= \vec{L}_n \\
\vec{N}' &= \vec{N}_n \\
\vec{P}' &= R_{\vec{N}_n} \left(2\pi \frac{T_e}{T_N} \right) \vec{P}_n \\
T_e &= 2\pi (-2E_e)^{-3/2} \\
T_N &= 2\pi (2BN_n)^{-1}
\end{aligned} \tag{2}$$

Here T_e and T_N represent the Keplerian period of the electron and the free rotation period of the core respectively, and $2B$ is the reciprocal of the moment of inertia of the core, according to usual molecular spectroscopy notation. Atomic units ($e = \hbar = m = 1$) are used throughout and the equations given simply follow from the elementary mechanical properties of Kepler motion and of free rotation.

- (ii) After the free motion, one has a “collision” of the electron with the core, when it is near enough to feel the anisotropic part of its potential. Due to cylindrical symmetry of this potential, the projection $\Lambda = \vec{L} \cdot \vec{P}'$ of \vec{L} on the molecular axis \vec{P}' is conserved. Again, as pointed out above, we assume that the magnitude of \vec{L} is conserved. This collision is thus described by a precession of \vec{L} around the molecular axis \vec{P}' by an angle $\delta\phi$. Due to invariance of the core potential in any plane containing the molecular axis \vec{P}' , $\delta\phi$ must be odd in $\theta \rightarrow \pi - \theta$. We take in the present paper the simplest choice $\delta\phi = K \cos \theta = K \vec{L} \cdot \vec{P}' / L$, which defines the coupling strength K . In equations, this leads to

$$\begin{aligned}
\vec{P}_{n+1} &= \vec{P}' \\
\vec{L}_{n+1} &= R_{\vec{P}'}(\delta\phi) \vec{L}' \\
\vec{N}_{n+1} &= \vec{J} - \vec{L}_{n+1}
\end{aligned} \tag{3}$$

It should be noted that the effects of the change in \vec{N} in the last equation are rather profound. First, and most important, there is an energetic consequence. This change involves a change in the magnitude N of \vec{N} and hence in the core kinetic energy $E_N = BN^2$. This in turn reflects itself in a change in $E_e = E - E_N$, which in turn, will affect both T_N and T_e in the following free motion. The system is therefore quite far from being a simple kicked top, in which the motion of \vec{L} would be decoupled from the rest of the dynamics. Second there is a kinematical consequence: since \vec{L} has rotated by $\delta\phi$ around \vec{P}' , and thus moved with respect to \vec{J} , this entails a reorientation of \vec{N} and, since the angle ϕ is defined with \vec{N} as reference axis (see fig. 1), this produces an extra $\delta\phi'$, which was called frame recoil in ref. [3]

In the Appendix B of this ref. [3] are given explicit expressions for the map established in molecular frame, which, even if less obvious to visualize, are easier to write down explicitly.

In any case what we shall be always presenting are the values of (θ_n, ϕ_n) describing the orientation of \vec{L} with respect to \vec{P}, \vec{N} , which are equally well defined in the laboratory frame or in a fixed molecular frame.

The most important consequence of this exchange of energy between electron and core is that if the total energy E is just slightly above the core energy for the lowest core angular momenta allowed, we will find points on this sphere, for which the electron energy E_e is positive and others for which it is negative. The positive electron energy region is thus given by $E > E_N = BN^2$, which using $J^2 = (\vec{L} + \vec{N})^2$ gives

$$BN^2 = B \left(-L \cos \alpha + \sqrt{J^2 - L^2 \sin^2 \alpha} \right)^2 < E \quad (4)$$

This condition depends only on the angle α between \vec{L} and the \vec{N} axis, so that the positive electron energy region is a cap about the positive \vec{N} - axis.

Therefore we can describe a scattering process by initiating the map with a point in the positive electron energy region and terminating it whenever we hit this region again. Indeed the restriction of the MQDT map to positive electronic energy has been identified [9] with the Jung scattering map [10,11]. Ionization processes would correspond to starting at some internal point and stopping when the positive energy region is hit for the first time.

3 Numerical Results

For the part of the sphere corresponding to negative electron energy, one observes the usual KAM scenario as the coupling constant K increases. The size of the ordered regions decreases as K grows. To get an idea of the general KAM structure in Fig. 2 we show views of the map at total energies E just above the ionization energy for two different coupling constants. Note that, for strong coupling, elliptic regions are (nearly) invisible. For the weaker constant these regions are large at the back of the sphere and display the typical features of a twist map. These elliptic regions correspond to positive (total) energy bound states, which are stable in the classical regime. In quantum mechanics we will expect them to decay slowly, and it will be interesting, in some future work, to study their decay law, which will not obviously be exponential, due to the fractal structure of islands surrounding the main elliptic islands.

We next proceed to analyze the time delays in scattering both for strong and weak coupling. Here we have to address the question whether we wish to look at the real time or at the number of iterations of the map. The real time

is certainly more attractive at first sight, but the excursions of the electron on a Rydberg orbit take times that approach infinity as the electron energy approaches zero from below. Not only do these long times distort the entire picture but they are actually also unrealistic because any electron will feel some perturbation on a sufficiently long excursion. We shall therefore first consider the delay in terms of iterations of the map in detail and at the very end show the true time evolution.

The most common idea nowadays to study these scattering delays would be to launch a set of trajectories on the circle corresponding to the scattering threshold, and to display the fractal structure of these delays as a function of the angle along this circle. As said in the introduction we saw no structure this way. To understand what is going on we use the following trick. Suppose that for some reason (e.g. external electric field) the electron is ionized for some negative electron energy E_e : this would correspond to suppress far flung trajectories. We can then launch a set of trajectories on this new threshold circle and study the new delays. We have done this for the same parameters as for all other cases in this paper (see the caption of table 1), which correspond to a very narrow cap of angle $\alpha_0 = 0.075\pi$ of positive electron energies, but selecting artificial ionizing thresholds electron energies which correspond to half sphere ($\alpha_0 = 0.5\pi$) and quarter sphere ($\alpha_0 = 0.25\pi$). The corresponding structure (delay versus angle β on the ring (see fig. 1)) is displayed on fig. 3. The half sphere case displays clearly the expected fractal delay structure (we have checked that it is indeed fractal by expanding some parts of this structure). For the narrower quarter sphere case the fractal structure becomes very narrow, and for the true zero energy ionization threshold it is no more visible.

We will thus now study the diffusion process, for which it will turn out as we will see that these far flung trajectories instead of being a drawback are an advantage because they are responsible of the interesting structure we will see.

Let us first consider the strong coupling case $K = -1$: Fig. 4 shows the time evolution of a set of 20000 incoming particles arranged on a ring concentric to the circle that defines the scattering threshold. The sequence shows the original distribution and its evolution after 1, 3, 10 and 100 iterations. Note that the total number of particles diminishes due to scattered particles. Thus the density diminishes but after a small number of iterations this density tends to be very uniform, i.e. the system has equilibrated. Note that the escaping particles are drawn as empty squares that appear on the cap of the sphere that corresponds to positive electron energies.

In Fig. 5 top, we show the number of particles escaping at a given iteration in a semi-logarithmic plot. We see the straight line characteristic of exponential decay dominating the figure, and an anomaly in the first channel. To get a

better feeling for this short time behavior, we next look at a log-log plot of the same data in Fig. 5 bottom. Here we see that the short time ($t \lesssim 10$) behavior is a straight line *i.e.* a power-law. Whereas the exponential behavior is standard for chaotic scattering, the power law for the transient is puzzling at first sight.

To gain better understanding we pass to the weak coupling case given by $K = -0.1$. Again we first look in Fig. 6 at a sequence of pictures after 1, 5, 1000, 10 000, iterations. Here we see that the particles diffuse very slowly towards the back of the sphere and they never penetrate the elliptic islands. At very large numbers of iterations some get quite close, and thus may penetrate the fractal tangle of small islands.

To get a quantitative understanding of the observed behavior, we again plot the number of escaping particles versus iteration in a log-log plot (fig. 7). We see an initial power law as in strong coupling for now roughly 1000 channels. This power law can now be accurately fitted to determine its power $-3/2$ (cf table 1). This result is compatible with the findings of fig. 5, -bottom

Furthermore in this weak coupling case an other distinct deviation from exponential behavior appears at very long times ($t \gtrsim 2 \cdot 10^5$). This last region is compatible with a power law between -1 and -3. Let us treat first this second power law. This is what we expect for particles caught in the chaotic tangle [12][13]. That this is indeed the effect we are seeing, can easily be shown as follows. In fig. 8 we see that some particles show regions in their time-evolution plot where the angle α between \vec{L} and \vec{N} does not change over many iterations indicating trapping in the fractal tangle around an island which has this behavior according to fig. 2. We may actually subtract these iterations and make a new plot of delays where these are absent as shown in Fig. 9. The final power law tail disappears, but the lower times region is not affected.

4 Diffusion Model

Let us focus now on the interpretation of this first power law, which is the most interesting part of our results. The law

$$At^{-3/2} \exp(-t/T) \tag{5}$$

corresponds, as is well-known, to the probability that a 1D random walk starting from the origin in an interval of length $L \sim \sqrt{T}$ returns to the origin for the first time at time t [14]. We could readily explain the connection to the Rydberg model by the following argument: Our map consists of two parts: during the long Rydberg excursion of the electron the core rotates around the \vec{N} axis

very often and we have to take the total rotation modulo 2π which makes for a reasonable randomizer of the rotation angle β . Yet the kick $\delta\phi = K \cos\theta$ produced in the orthogonal direction (around \vec{P}) depends on the final value of this angle β . In particular it is towards the front or back of the sphere depending whether this \vec{N} rotation left it on the upper $z > 0$ or lower $z < 0$ part of the sphere. It thus becomes a random walk towards the front or back of the sphere. This could explain our findings. However there is a distinct qualitative difference between this 1D random walk law and our Rydberg results. It is displayed by comparing the previous fig. 9 with the theoretical fig. 10. Indeed, the law (5) always leads to a value that is lower than the corresponding power law $At^{-3/2}$, whereas in our Rydberg case there is a long, nearly horizontal, shoulder between the power law and the exponential decay. Mathematically the two histograms, (7) and (9) for the Rydberg case can be fitted by a formula

$$\left(A_1 t^{-\alpha_1} + A_2\right) \exp(-t/T) + A_3 t^{-\alpha_3} \quad (6)$$

with $A_3 = 0$ for the latter case. Parameters are given in table 1. There are negligible residuals: the sluggish transition between the two parts is an effect of non additivity in a log-log plot, and there is no statistically significant possibility to fit two independent time constants for A_1 and A_2 . This introduces a second characteristic time,

$$t_c = (A_1/A_2)^{1/\alpha_1}, \quad (7)$$

which is the transition time between power law and exponential regimes, besides the time constant of the exponential decay T , which is much longer. The time t_c has no equivalent in the 1D random walk model. In both strong and weak coupling cases t_c corresponds roughly according to figs. 4 and 6 to the time needed for the particles to fill two thirds of the sphere.

To check these ideas we replace the true rotation $\delta\beta$ by a random one, equidistributed on $[0, 2\pi)$, while keeping the exact Rydberg formula for the collisional kick $\delta\phi + \delta\phi'$ and resulting $\delta\alpha$, which is the significant parameter to monitor distance to ionization. The result (fig. 11 and table 1) is virtually indistinguishable from the case where trapped parts of trajectories are eliminated (fig. 9). Since in this case the regular part at the back of the sphere has disappeared (see fig. 12), this result first corroborates our previous conclusion that the long time tail is due to trajectories trapped in the chaotic tangle. Second it shows that the model of random β is correct but that the right Rydberg value of the kick $\delta\phi + \delta\phi'$ introduces a qualitative difference with respect to the simple model of a constant amplitude kick. To gain further insight, since the formula for $\delta\phi + \delta\phi'$ is too complex to enable to visualize easily its effects, we compute

a first order development of $\delta\alpha$ as a function of the small parameter K :

$$\delta\alpha = \left(1 - \frac{L}{\sqrt{J^2 - L^2 \sin^2 \alpha}} \cos \alpha\right)^{-1} \frac{1}{2} K \sin \alpha \sin 2\beta \quad (8)$$

Neglecting the recoil $\delta\phi'$, which is valid if $L \ll J$, it simplifies further as:

$$\delta\alpha = \frac{1}{2} K \sin \alpha \sin 2\beta \quad (9)$$

With any of these first order formulas, the resulting histogram (fig. 13 and table 1) corresponds to the 1D random walk prediction of Eq. (5) and fig. 10, with no exponential shoulder. What is characteristic in these equations is that for an equipartition of β on $[0, 2\pi)$ the average value of $\delta\alpha$ is zero. The exact value of the law, especially the way it varies with α is of little importance. This is expected since a variation of $|\delta\alpha|$ with α can be compensated for by a renormalisation of α to keep its variation constant on average. The existence of the exponential shoulder is thus related to the fact that the true $\delta\alpha$ is not zero on average. This is shown by writing $\delta\alpha$ up to second order in K (neglecting $\delta\phi'$ to simplify):

$$\delta\alpha = \frac{1}{2} K \sin \alpha \sin 2\beta + \frac{1}{4} K^2 \sin 2\alpha \sin^4 \beta. \quad (10)$$

The resulting histogram (fig. 14) displays indeed the exponential shoulder. The explanation is as follows. The average value of $\delta\alpha$ is positive for the front part of the sphere ($0 < \alpha < \pi/2$), thus pushing it backwards towards the middle (increasing α), and conversely negative for the back part of the sphere, pushing it also towards the middle. This creates a kind of trap in the middle of the sphere, and the exponential law results from the need to escape that trap.

To justify this explanation let's put it quantitatively. We first renormalize α to have constant average $|\delta\alpha|$ by redefining a new coordinate

$$x = \frac{1}{2} \ln \frac{1 + \cos \alpha}{1 - \cos \alpha} \quad (11)$$

which varies between $-\infty$ and $+\infty$ when α varies between π (back) and 0 (front of the sphere). x has been computed so that to first order δx is independent of x , and then to second order in K

$$\begin{aligned} \delta x &= -\frac{1}{2} K \sin 2\beta - \frac{1}{2} K^2 \cos \alpha \left(\sin^4 \beta - \frac{1}{4} \sin^2 2\beta \right) \\ &= -\frac{1}{2} K \sin 2\beta - \frac{1}{2} K^2 \tanh x \left(\sin^4 \beta - \frac{1}{4} \sin^2 2\beta \right) \end{aligned} \quad (12)$$

We obtain thus a random motion with differing average amplitude in the two directions. This is equivalent to a thermal motion within a potential $V(x)$. The average step is $\pm K/2\pi$ and the difference between the two directions comes from a Boltzmann factor:

$$\exp(-V'(x) \times K/\pi) \simeq 1 - V'(x) \times K/\pi = \frac{\langle \delta x^+ \rangle}{\langle \delta x^- \rangle} = 1 - \frac{\pi}{4} K \tanh x, \quad (13)$$

where we have normalized temperature and potential so that $kT = 1$. Thus

$$V(x) = \frac{\pi^2}{4} \ln \cosh x \quad (14)$$

This potential is plotted in fig. 15. The potential curve is limited on the right at the actual value of x corresponding to the ring of ionization in all preceding figures. The depth of the trap is 3.6, justifying a long time exponential to escape it.

In order to compare the results given here with the times reported in table 1, one should note the following: these times are given in number of iterations. However, at each iteration, x changes by an amount of order K , so that the natural diffusive time scale, over which x varies by a quantity of order one, is of order K^{-2} . We therefore expect the times given in table 1 to contain an overall factor of order K^{-2} apart from the first passage probability. That this is indeed so, is verified in the case $K = 0.2$, for which all times are approximately four times shorter than for $K = 0.1$.

The physical origin of this potential is obvious. The electron can both gain or loose energy at each collision with the core. The most probable situation is equipartition of energy, i.e. the middle of the sphere, and ionization which needs nearly all energy in the electron is a rather improbable situation. This potential takes thus into account the amount of available phase space.

We now give a theory of this phenomenon. We wish to solve the following problem: if we introduce a particle at the point a and this particle diffuses under the influence of a binding potential $V(x)$, what is the probability that it returns to a for the first time at time t , if the potential is of such a nature that being at the position a has quite a small probability in equilibrium? We shall show that in these circumstances it is to be expected on quite general grounds that this probability has the behavior outlined above, namely a $t^{-3/2}$ initial decay, followed by a plateau and finally ending in an exponential decay. At the intuitive level, this can be seen as follows: Near a , the process can be viewed as a diffusion with a drift away from a . This means that the distribution of first return times is of the type $t^{-3/2} e^{-t/t_e}$. This distribution, however, is not normalized to one, and the missing probability corresponds to particles

that diffuse away to infinity. These particles, however, will not really diffuse to infinity, but rather reach the equilibrium distribution $\exp(-V(x))$. Under these circumstances, it will from then on reach a at a rate $\exp(-V(a))$. This therefore yields an exponential decay in the first passage probability on a time scale T much larger than t_c , hence yielding the expected plateau. A more formal derivation is found in the Appendix.

5 Final Remarks

We finally display the true time delays in the two cases of strong and weak coupling, that is, we compute the actual time of each Rydberg excursion. We note in Fig. 16 that the different regimes detected in the iteration plots become quite blurred. This is due to the fact that two very similar trajectories near threshold have greatly different excursion times as the latter diverge at this threshold. The first consequence is that time curves span only two orders of magnitude whereas iteration curves span eight orders of magnitude. The first channel in the strong case and the first isolated peak in the weak coupling case correspond to electrons which are stabilized in the first collision and ejected exactly in the second. These features depend very critically on the exact position with respect of threshold of the incident ring of particles, whereas the remaining of the picture as well as iteration curves are stable against such minor variations. The $t^{-3/2}$ behavior in the weak coupling case corresponds only to a longer decreasing plateau, the slope of which is no more 1.5. The delay between $t^{-3/2}$ and exponential decay is no more visible, and finally the last t^{-n} decay has also disappeared. If we want to obtain information about the process, we conclude that the true time delays do not yield this information in a clear cut fashion.

We may conclude that our model displays typical properties of compound behavior in many respects. Yet the remarkably complicated structure of the time delay indicates that more information can be obtained than is commonly assumed e.g. in nuclear compound reactions. The diffusive model seems promising, as it can readily describe situations where the regimes are not as clearly separated, which may be more common.

As our analysis is limited to classical mechanics it remains an interesting open question, how this situation translates to quantum mechanics. Also one will have to ask what features are very model dependent and what features may be found in more general context. In particular we think about the possibility of a diffusive description of pre compound situations.

A Appendix

In this Appendix, we shall show at a more formal level that the behavior of the type described in the text is quite general for first return probabilities in a potential that goes to infinity when $|x| \rightarrow \infty$. The master equation satisfied by the probability $P(x, t)$ of reaching x at time t is given by

$$\frac{\partial P(x, t)}{\partial t} = \frac{\partial}{\partial x} \left[\frac{\partial P}{\partial x} + V'(x)P \right] \equiv -LP, \quad (\text{A.1})$$

where the last equality defines the operator L . Here the initial condition is given by

$$P(x, 0) = \delta(x - a). \quad (\text{A.2})$$

From this one obtains

$$P(a, t) = \sum_{m=0}^{\infty} \frac{|\phi_m(a)|^2}{\phi_0(a)} e^{-E_m t}, \quad (\text{A.3})$$

where E_n and $\phi_n(x)$ are the eigenvalues and eigenfunctions of L respectively. The division by $\phi_0(a)$ is related to the fact that L is not self-adjoint with respect to the ordinary scalar product, so that the $\phi_n(x)$ are not orthogonal. However, replacing $\phi_n(x)$ by $\phi_n(x)/\sqrt{\phi_0(x)}$ restores self-adjointness.

As is well-known, the Laplace transform $Q(s)$ of the first passage probability $q(t)$ is given by[14]

$$Q(s) = \frac{P(s)}{1 + P(s)}, \quad (\text{A.4})$$

where $P(s)$ is the Laplace transform of $P(a, t)$ given by (A.3).

Now we need both a large and a small time estimation for the expression (A.3). The large time estimate is trivial: Since (A.1) always has an equilibrium solution, L always has a zero eigenvalue. At large times, this eigenvalue always dominates, and one has

$$P(a, t) = \phi_0(a) = e^{-V(a)}. \quad (\text{A.5})$$

For short times, on the other hand, one may simply assume that the diffusing particle does not go far from a , so that we replace $V(x)$ by its Taylor

development to first order. Then (A.1) can be solved exactly to yield

$$P_d(s) = \frac{1}{\sqrt{4s + V'(a)^2}}, \quad (\text{A.6})$$

where $P_d(s)$ is the approximation to $P(s)$ in this approximation. From (A.3) follows, however, that $P(a, t)$ is never less than $\phi_0(a)$, which we may incorporate approximately by setting

$$P(s) = P_d(s) + \frac{\phi_0(a)}{s}. \quad (\text{A.7})$$

From this follows

$$Q(s) = \frac{\phi_0(a)\sqrt{4s + V'(a)^2} + s}{(s + \phi_0(a))\sqrt{4s + V'(a)^2} + s}. \quad (\text{A.8})$$

If $s \ll V'(a)^2$, this reduces to a rational function in s , which corresponds to a double exponential decay, with decay times τ_1 and τ_2 approximately given by

$$\tau_1 = \frac{2}{V'(a)(1 + V'(a))} \quad \tau_2 = \frac{1 + V'(a)}{\phi_0(a)V'(a)} \quad (\text{A.9})$$

The τ_2 decay clearly dominates the picture at those times. Since τ_2 is much larger than the time at which this approximation starts to be valid, namely approximately $V'(a)^{-2}$, this implies the existence of the plateau followed by an exponential decay. On the other hand, in the large s approximation we may altogether neglect the correction made in (A.7) and use $P_d(s)$. This yields

$$Q(s) = \frac{1}{\sqrt{4s + V'(a)^2} + 1}, \quad (\text{A.10})$$

which yields a $t^{-3/2}$ decay cut off by an exponential at a time scale of order $V'(a)^{-2}$. This meshes therefore quite well with the large time asymptotics, which just then begins to set in.

References

- [1] M. J. Seaton, Quantum defect theory, Rept. Progr. Phys. 46 (1983) 167–257.

- [2] U. Fano, Quantum defect theory of ℓ uncoupling in H_2 as an example of channel-interaction treatment, *Phys. Rev. A* 2 (1970) 353–365.
- [3] M. Lombardi, P. Labastie, M. C. Bordas, M. Broyer, Molecular Rydberg states: classical chaos and its correspondence in quantum mechanics, *J. Chem. Phys.* 89 (6) (1988) 3479–90.
- [4] M. Lombardi, T. H. Seligman, Universal and nonuniversal statistical properties of levels and intensities for chaotic Rydberg molecules, *Phys. Rev. A* 47 (5) (1993) 3571–86.
- [5] M. Lombardi, J.-P. Pique, P. Labastie, M. Broyer, T. Seligman, Chaos in molecules by statistical Fourier transform spectroscopy, *Comm. At. Mol. Phys.* 25 (4-6) (1991) 345–57.
- [6] F. Benvenuto, G. Casati, D. L. Shepeliansky, Chaotic autoionisation of molecular Rydberg states, *Phys. Rev. Lett.* 72 (12) (1994) 1818–1821.
- [7] R. Neuhauser, K. Siglow, H. J. Neusser, Hydrogenlike Rydberg electrons orbiting molecular clusters, *Phys. Rev. Lett.* 80 (23) (1998) 5089–5092.
- [8] U. Even, R. D. Levine, R. Bersohn, Observations of molecular Rydberg state decay for $n = 10$ -200, *J. Phys. Chem.* 98 (13) (1994) 3472–3477.
- [9] B. Dietz, M. Lombardi, T. H. Seligman, Parabolic manifolds in the scattering map and direct quantum processes, *J. Phys. A (Math. Gen.)* 29 (5) (1996) L95–9.
- [10] C. Jung, Poincaré map for scattering states, *J. Phys. A* 19 (1986) 1345.
- [11] C. Jung, T. H. Seligman, Integrability of the S -matrix versus integrability of the hamiltonian, *Phys. Rep.* 285 (1997) 77–142.
- [12] G. Casati, G. Maspero, D. L. Shepelyansky, Quantum Poincaré recurrences, *Phys. Rev. Lett.* 82 (1999) 524–527.
- [13] B. V. Chirikov, D. L. Shepelyansky, Asymptotic statistics of Poincaré recurrences in hamiltonian systems with divided phase spaces, *Phys. Rev. Lett.* 82 (1999) 528–531.
- [14] G. H. Weiss, *Aspects and Applications of the Random Walks (Random Materials and Processes)*, North Holland, Amsterdam, 1994.

List of Tables

Table 1

DIFFUSION PARAMETERS. For all figures and this table: $L = 50$, $J = 100$, $E = +1.275 \cdot 10^{-7}$, $2B = 10^{-10}$, initial ring radius $\alpha_0 = 0.0725\pi$, $n = 10^7$ iterations. (a) Full Rydberg Case, (b) Eliminating trapped parts of trajectories, (c) Random β with true Rydberg $\delta\phi + \delta\phi'$, (d) Random β with first order $\delta\alpha$, no $\delta\phi'$. (e) Random β with $\delta\alpha$ up to second order in K , no $\delta\phi'$. (f) Idem including $\delta\phi'$. $t_c = \left(\frac{A_1}{A_2}\right)^{1/\alpha_1}$
 Between parentheses: one standard deviation on the last figure.

	K	α_1	T	$10^{-6}A_1$	A_2	t_c
(a)	0.1	1.594(2)	18735(110)	5.55(4)	70.0(6)	1184
	0.2	1.779(7)	5235(83)	6.33(7)	397(9)	270
	1	2.299(3)	453(1)	4.72(1)	13685(28)	13
(b)	0.1	1.604(4)	16061(225)	5.55(4)	83(2)	1018
(c)	0.1	1.589(2)	21844(65)	5.50(3)	58.8(4)	1344
(d)	0.1	1.532(2)	4748(70)	3.43(2)		
(e)	0.1	1.620(2)	34320(85)	4.27(3)	12.8(1)	2566
(f)	0.1	1.641(1)	19759(40)	4.31(1)	39.8(1)	1169

List of Figures

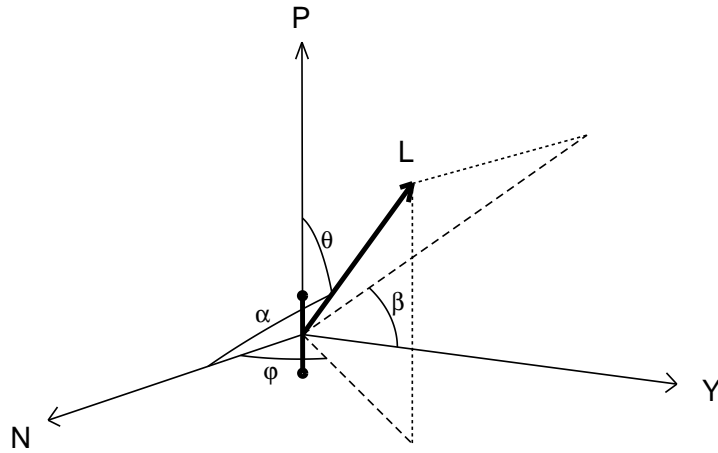


Fig. 1. Rydberg molecule reference frame.

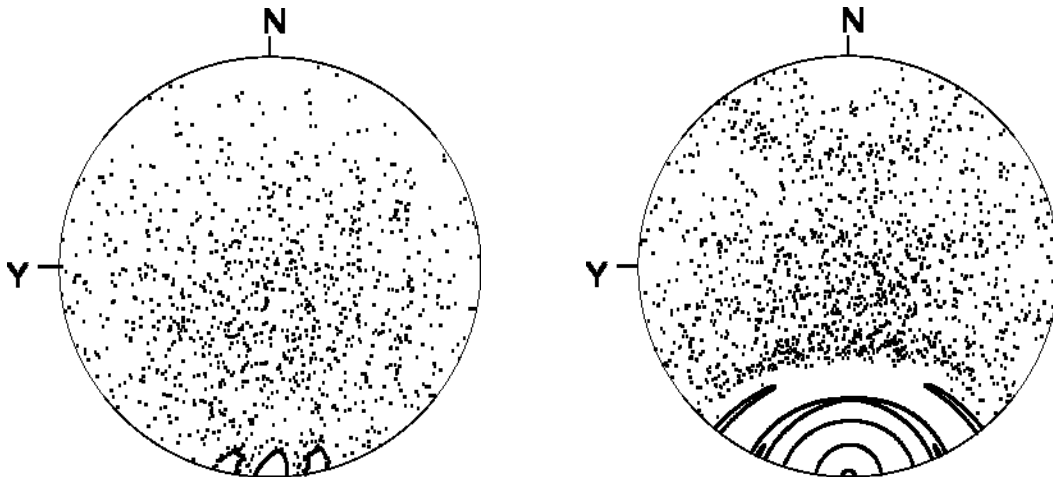


Fig. 2. Poincaré surfaces of section. Stereographic projection from pole \vec{P} . The positive electron energy region is a small (white) cap around positive \vec{N} , with angular radius $\alpha_0 = 0.075\pi$. Left: strong coupling ($K = 1$). Right: small coupling ($K = 0.1$).

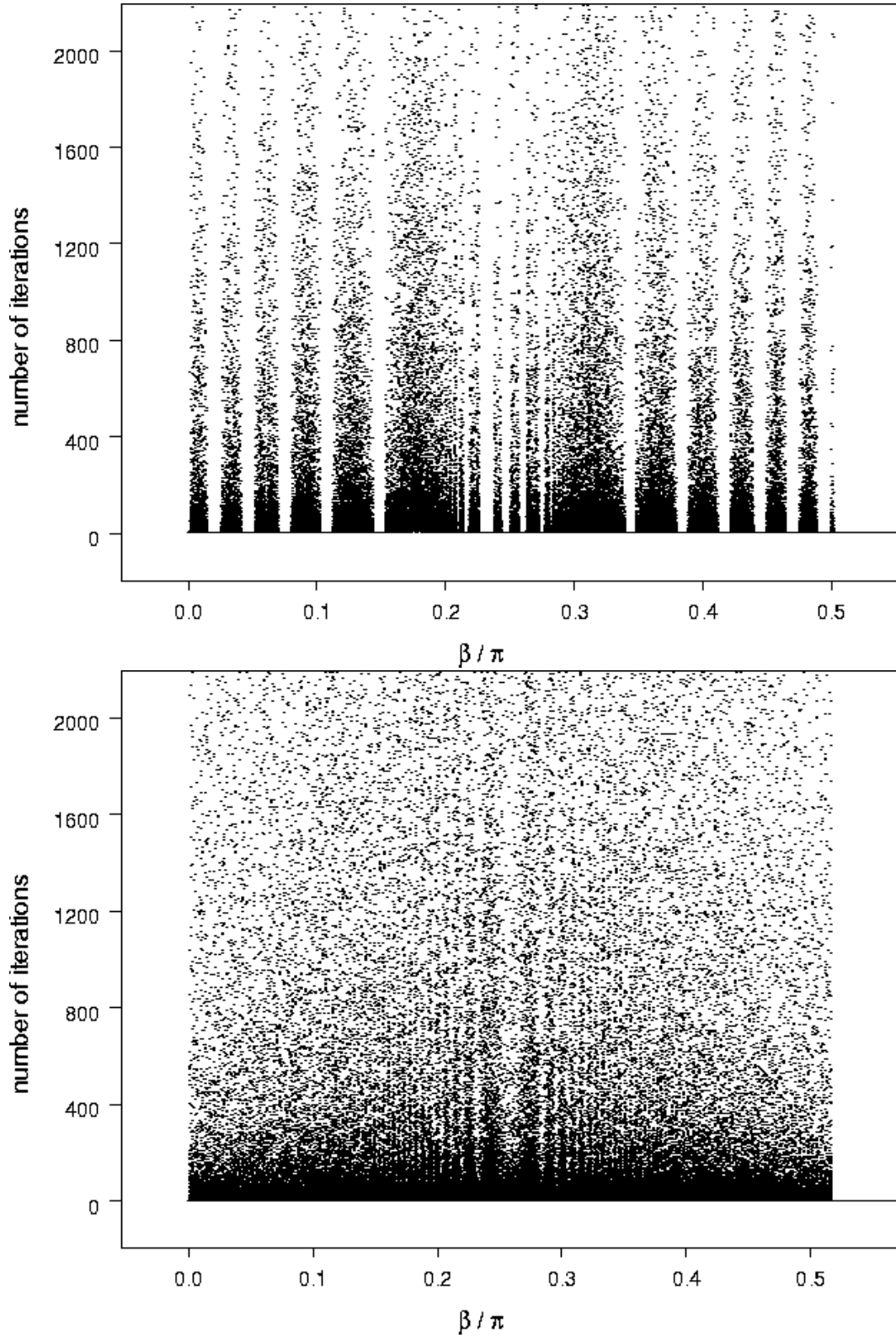


Fig. 3. Fractal structure of delays corresponding to artificial ionizing thresholds. Top: artificial threshold $\alpha_0 = 0.5\pi$. Bottom $\alpha_0 = 0.25\pi$. For actual zero energy threshold the structure becomes too narrow to be seen.

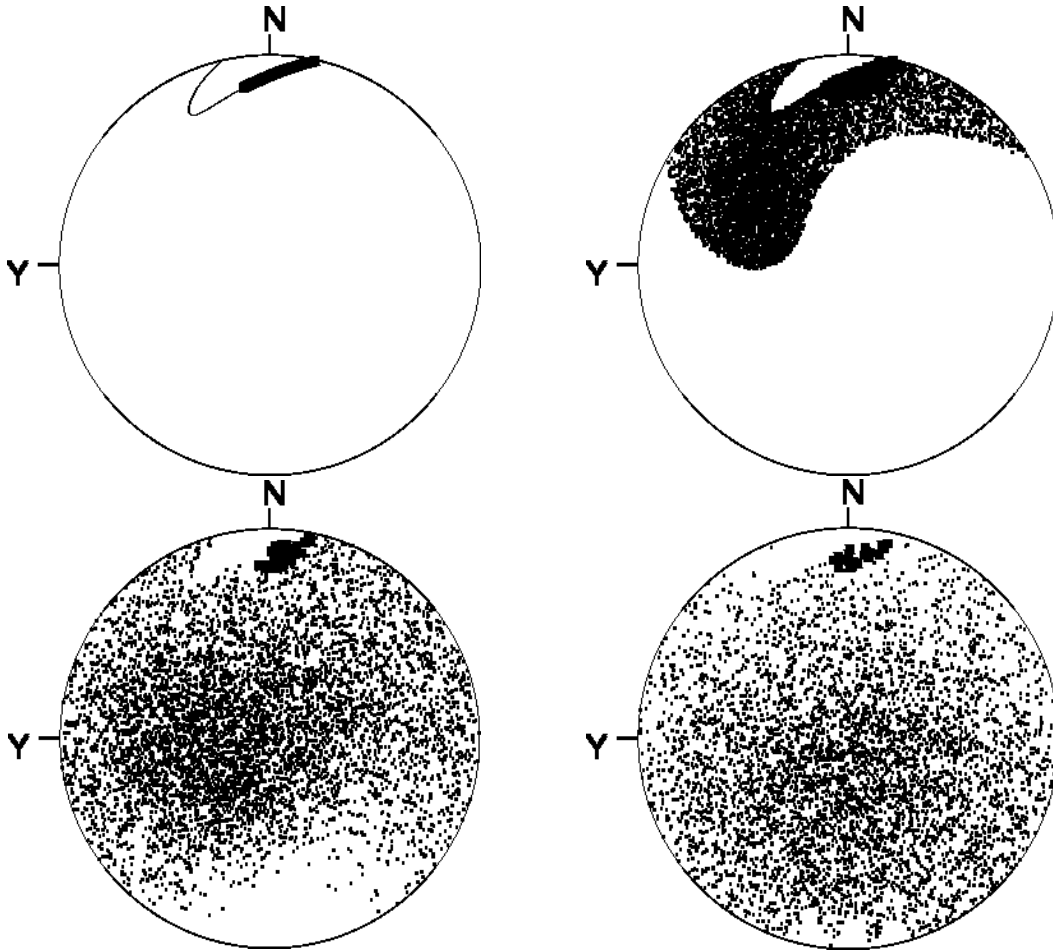


Fig. 4. Time evolution of a set of 20000 incoming particles arranged on the circle that defines the scattering threshold: large squares correspond to escaping particles. Strong coupling: $K = -1$. Top left: after 1 iteration (it): half the incoming particles are slowed down by the collision with the core and enter the sphere, half are accelerated and escape. Top right: idem after 3 it. Bottom left : after 10 it ($\sim t_c$ defined by Eq. (7)). Bottom right: idem after 100 it.

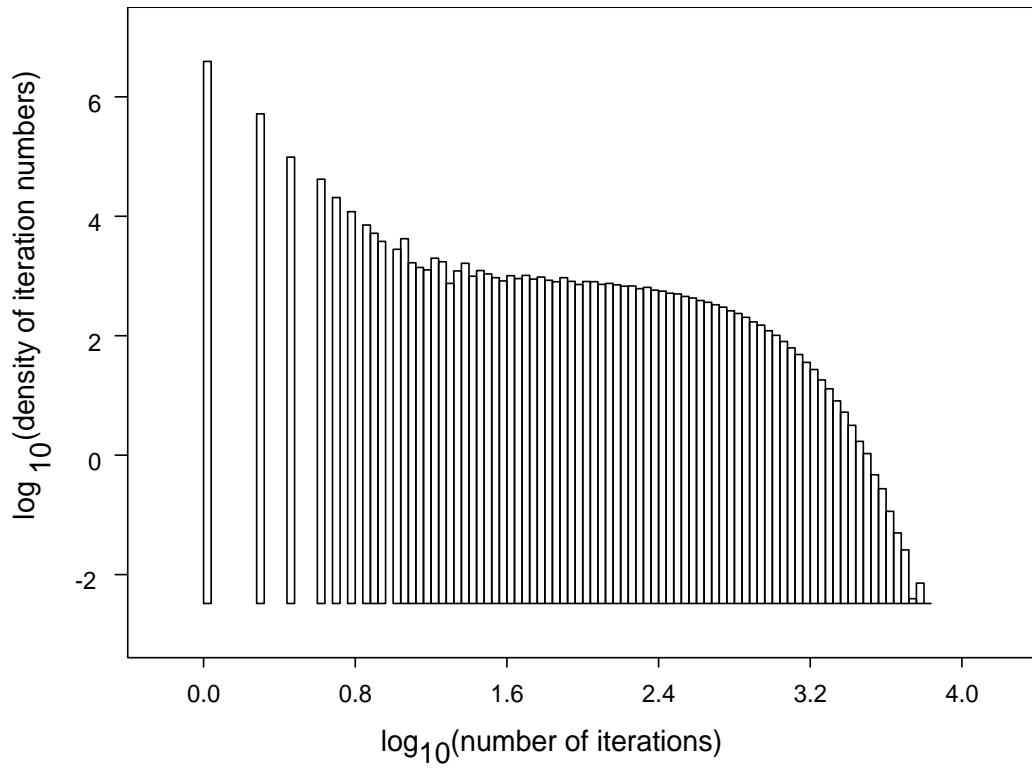
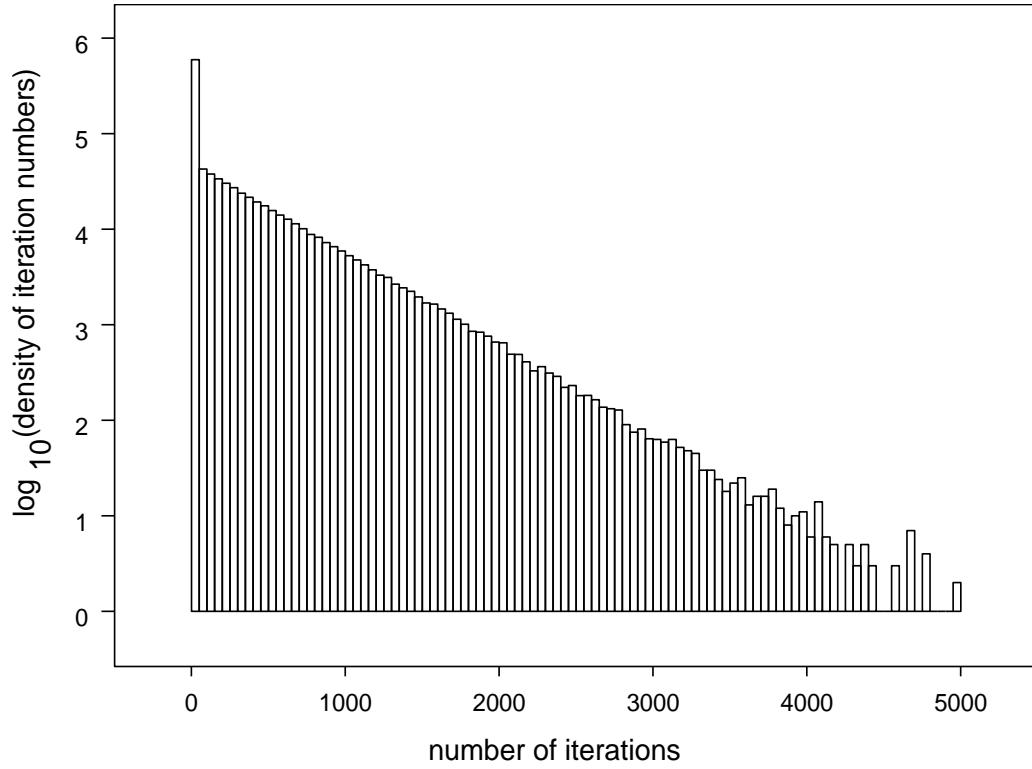


Fig. 5. Distribution of the number of iterations before escape. Strong coupling $K = -1$. Top: semi logarithmic plot, bottom: log log plot.

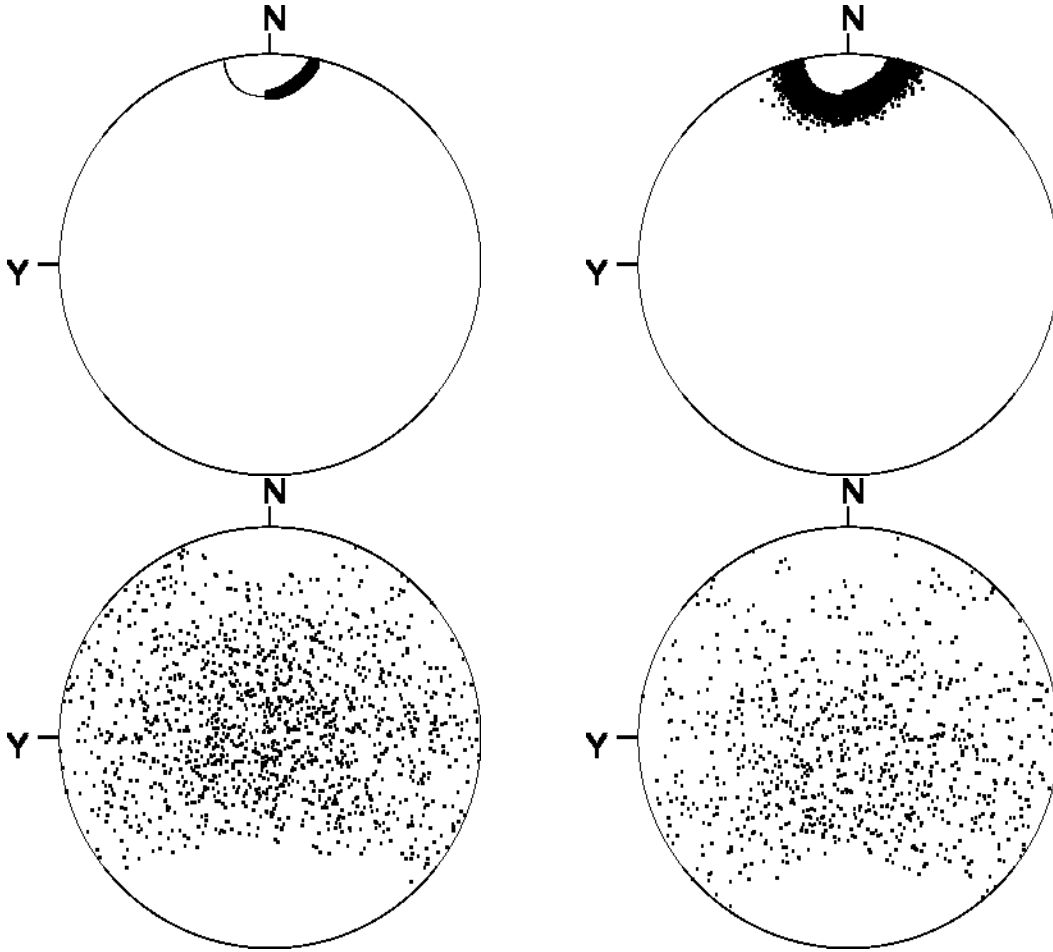


Fig. 6. Time evolution of a set of 20000 incoming particles arranged on a ring concentric to the circle that defines the scattering threshold: large squares correspond to escaping particles. Weak coupling: $K = -0.1$. Top left: after 1 iteration (it). Top right: idem after 10 it. Bottom left: after 1000 it ($\sim t_c$ defined by Eq. (7), see table 1). Bottom right: idem after 10 000 it.

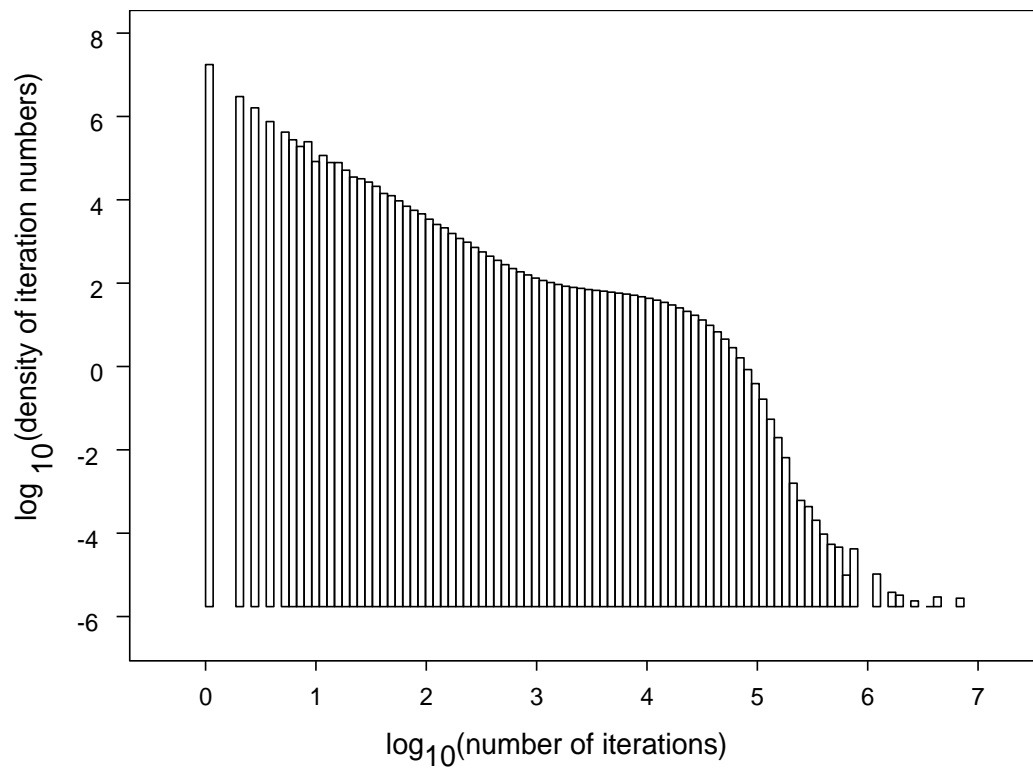


Fig. 7. Distribution of the number of iterations before escape. Log log plot, weak coupling $K = -0.1$.

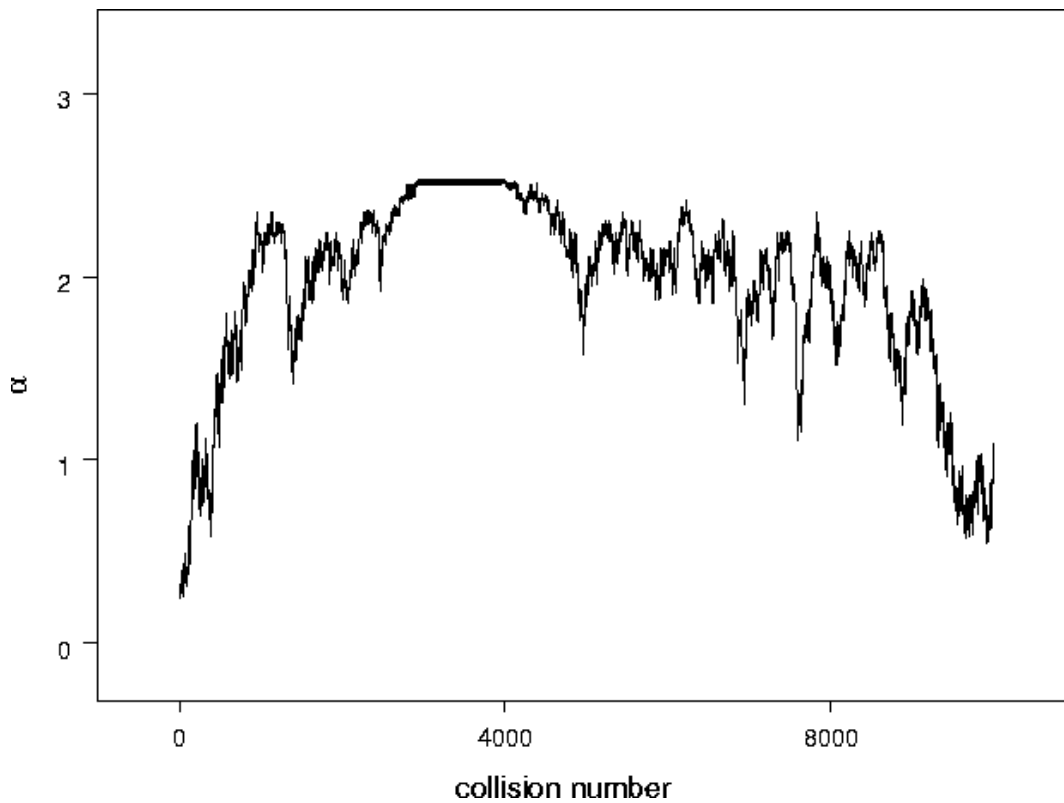


Fig. 8. Some particles are caught in the chaotic tangle: for a number of iterations α remains nearly constant at a value corresponding to the chaotic tangle (cf Fig. 2). Weak coupling $K = -0.1$.

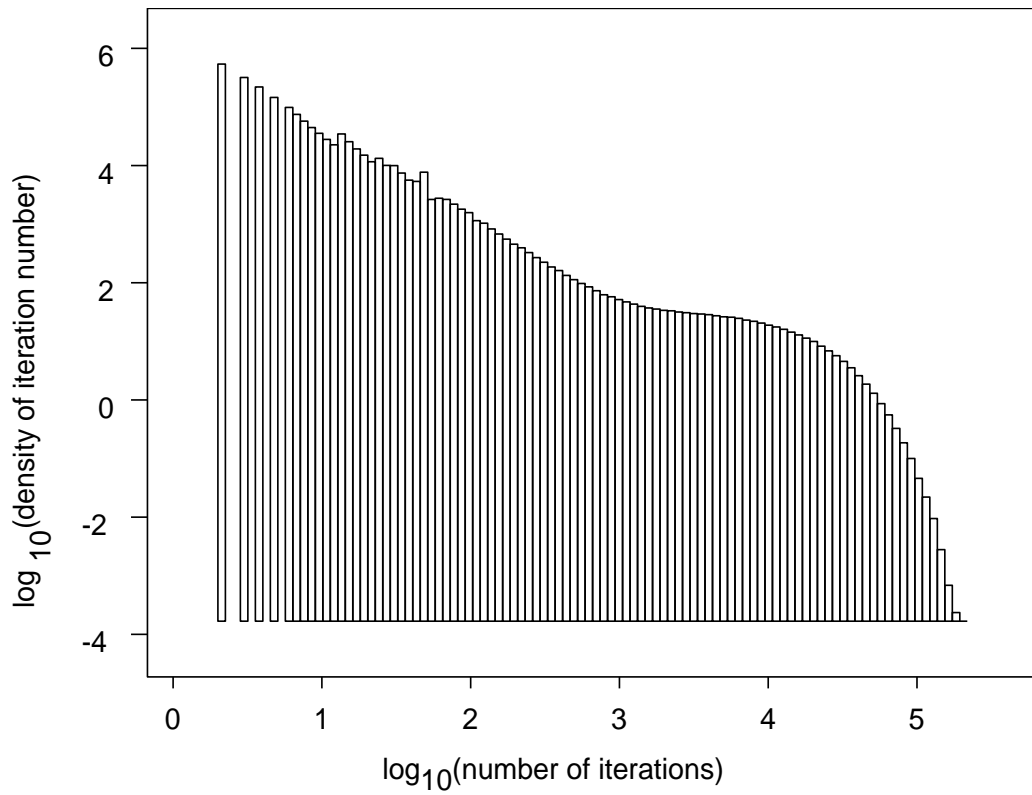


Fig. 9. Distribution of the number of iterations before escape, eliminating the iterations caught in the chaotic tangle. Weak coupling $K = -0.1$. Log log plot.

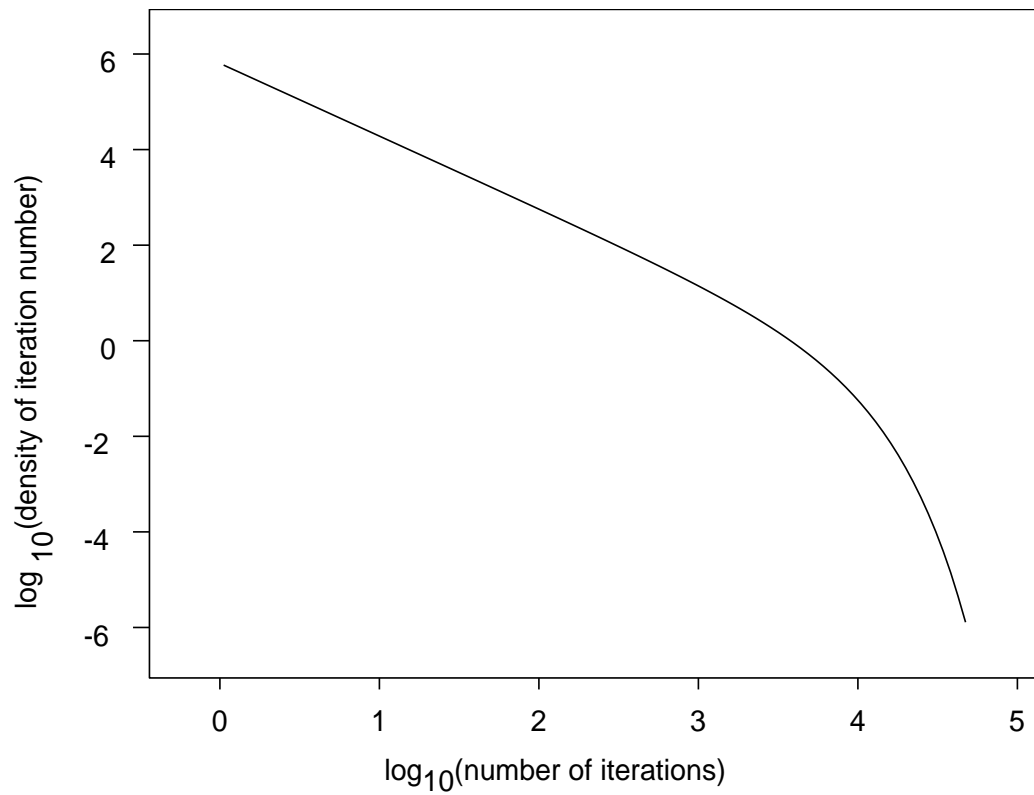


Fig. 10. Theoretical power law for a random walk in 1 dimension Eq. (5). Log log plot.

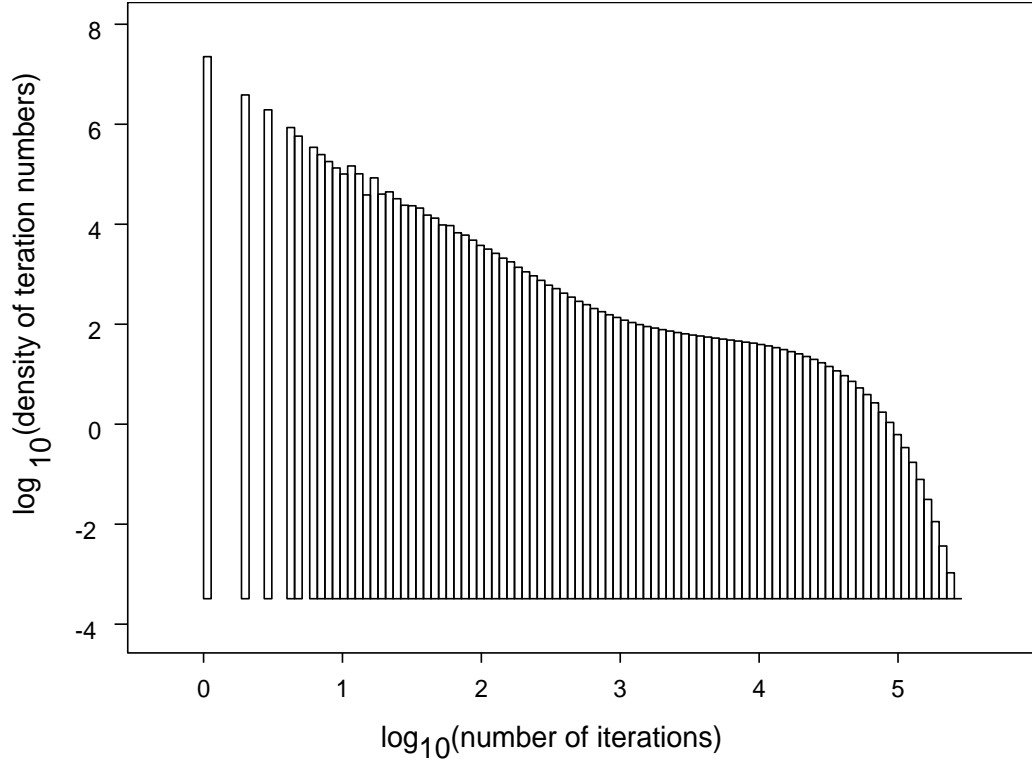


Fig. 11. Distribution of the number of iterations before escape, replacing the true $\delta\beta$ by a random one, while keeping the true Rydberg $\delta\phi + \delta\phi'$. The long time tail has disappeared, but the exponential regime remains in addition to the power law. Weak coupling $K = -0.1$.

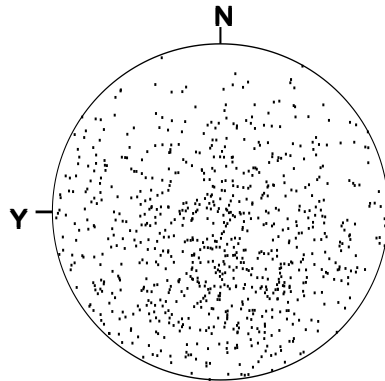


Fig. 12. Time evolution of a set of 20000 incoming particles arranged on a ring concentric to the circle that defines the scattering threshold, with random $\delta\beta$ and true Rydberg $\delta\phi + \delta\phi'$. Picture after 10 000 iterations. With respect to the last of figs. 6 the blank part at the bottom of the sphere which corresponds to the regular region has disappeared. Weak coupling: $K = -0.1$.

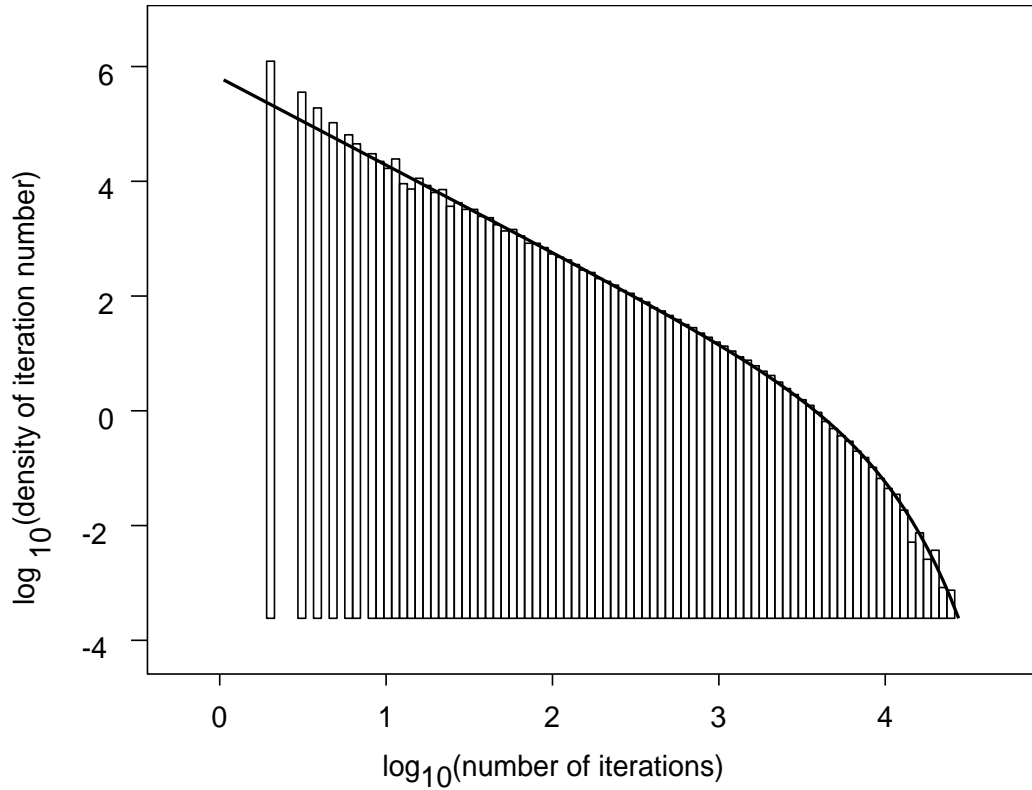


Fig. 13. Distribution of the number of iterations before escape, replacing the true $\delta\beta$ by a random one, and the true $\delta\alpha$ by the first order (in K) value of Eq. (9). Heavy line: fit by Eq. (5), with parameters given in table 1. Weak coupling $K = -0.1$.

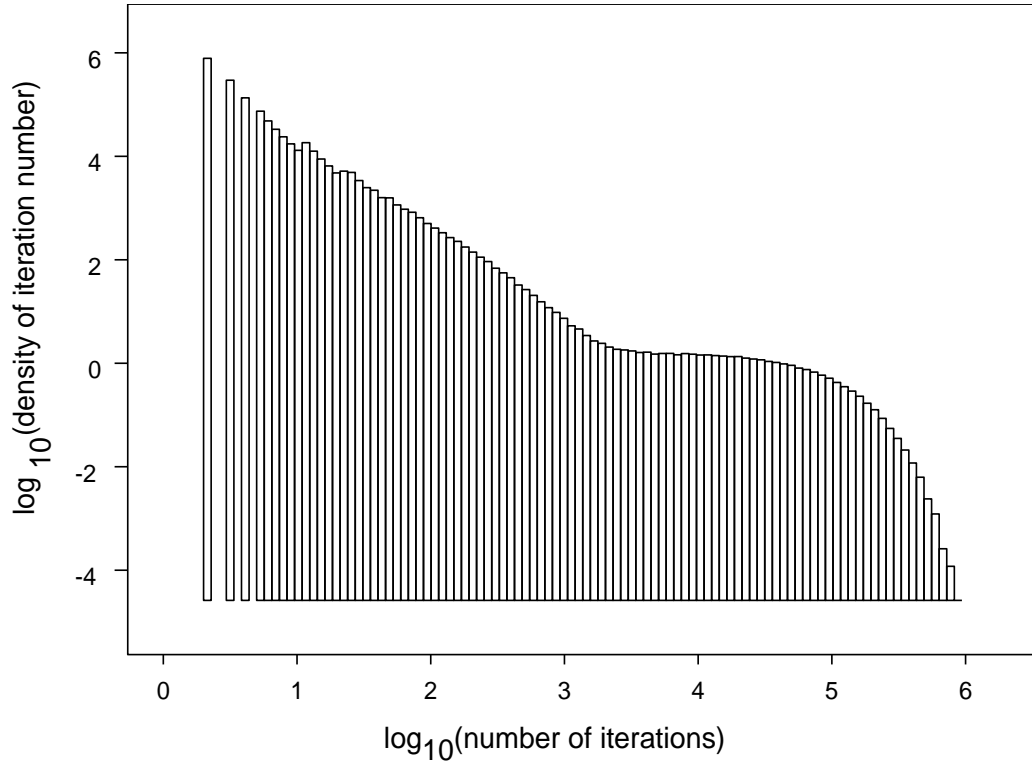


Fig. 14. Distribution of the number of iterations before escape, replacing the true $\delta\beta$ by a random one, and the true $\delta\alpha$ by the second order (in K) value of Eq. (10). Weak coupling $K = -0.1$.

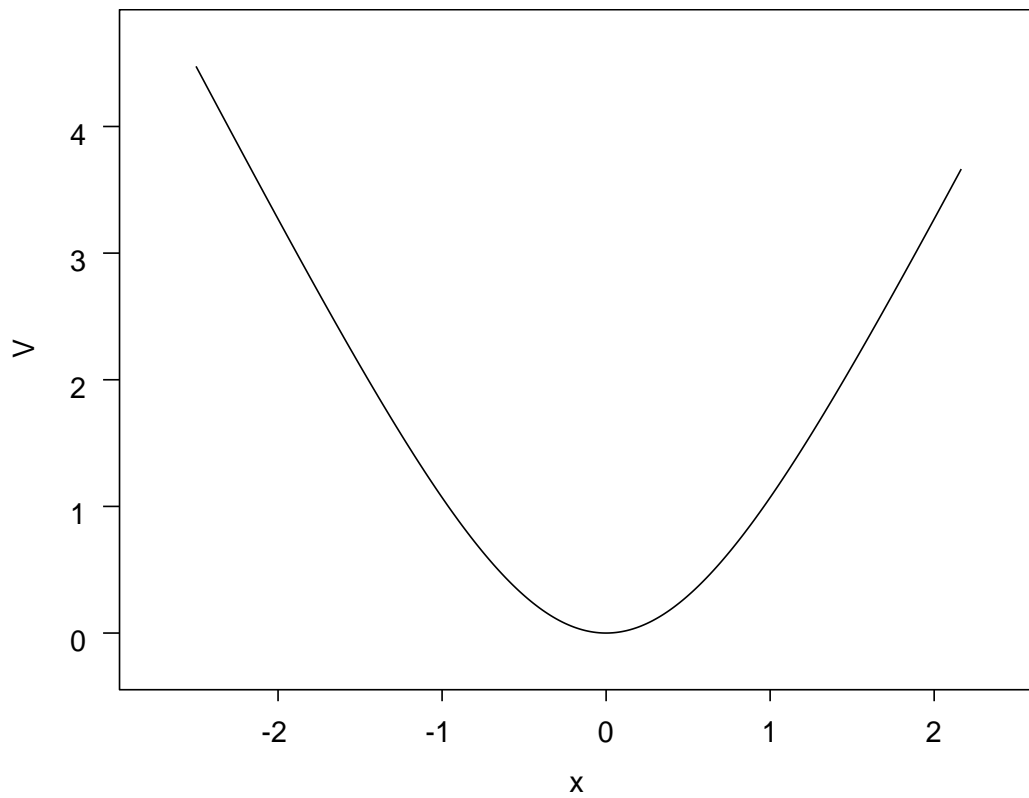


Fig. 15. Effective potential defined in Eq. (14). Ordinate unit is kT .

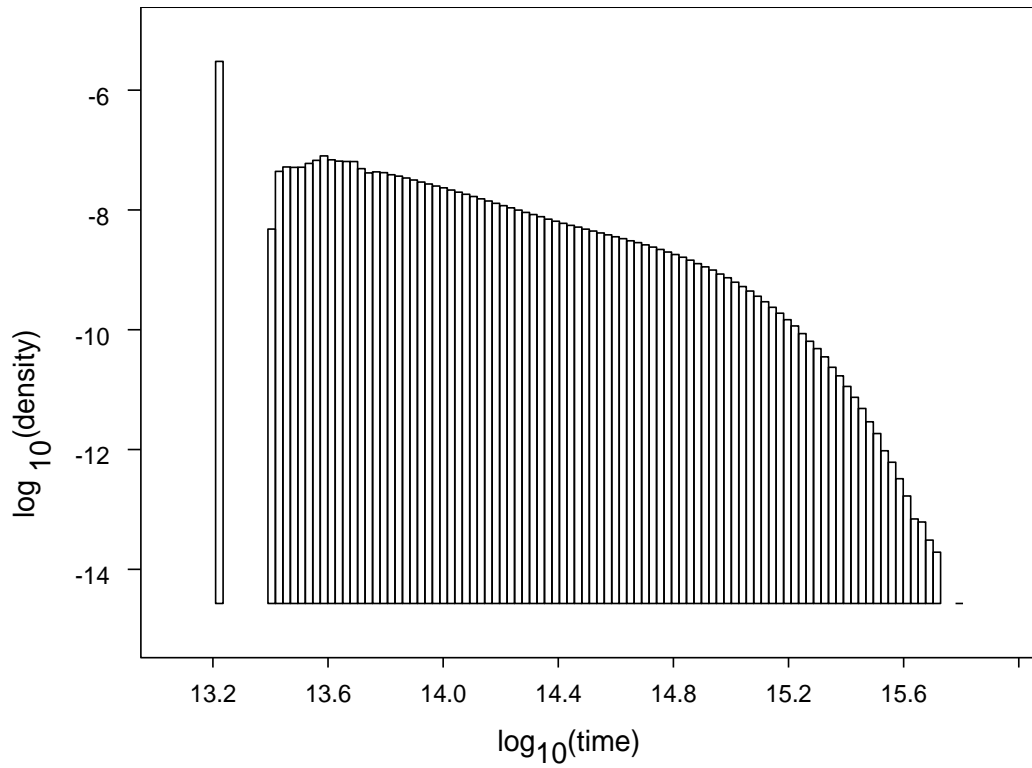
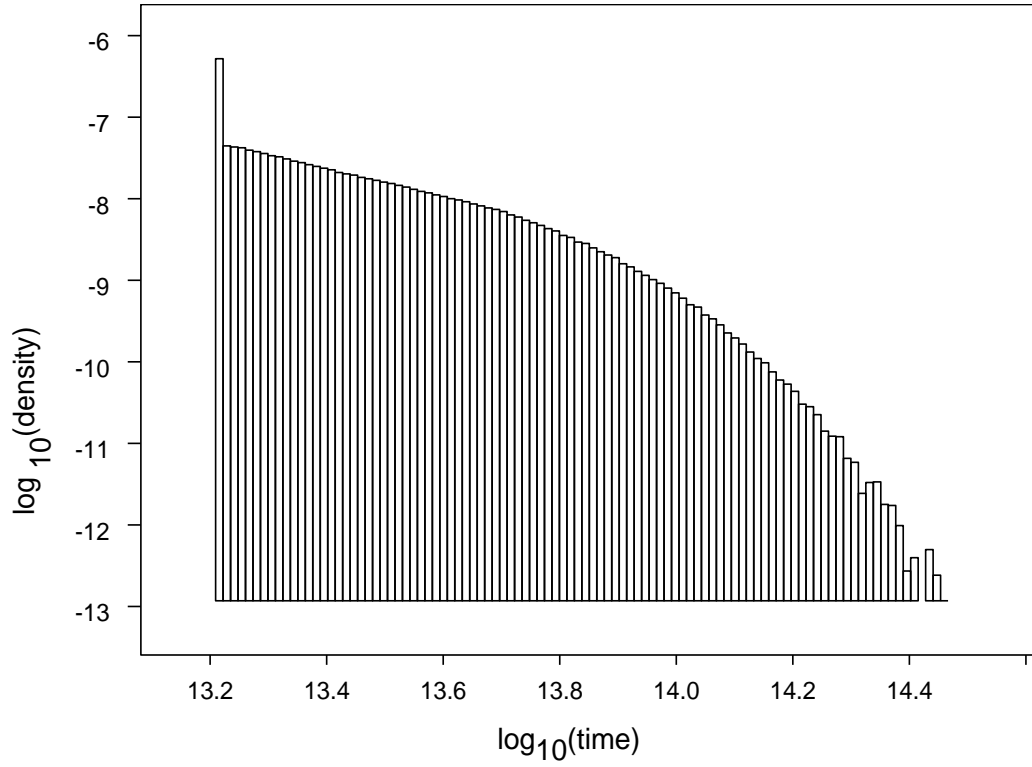


Fig. 16. True time delays. Log Log plot. Top: strong coupling, bottom: weak coupling.